DOI: 10.17725/rensit.2023.15.317

Holographic Method for Localization of a Moving Underwater Sound Source in the Intense Internal Waves Presence

Venedikt V. Kuz'kin

Prokhorov Institute of General Physics, Russian Academy of Sciences, http://www.gpi.ru/
Moscow 119991, Russian Federation
E-mail: kumiov@yandex.ru

Sergey A. Pereselkov, Sergey A. Tkachenko, Nikolay V. Ladykin, Mikhail V. Kutsov

Voronezh State University, http://www.vsu.ru/
Voronezh 394006, Russian Federation
E-mail: pereselkov@yandex.ru, sega-th@mail.ru, ladykin.edu@yandex.ru, mkutsov.edu@yandex.ru

Vladimir I. Grachev

Kotelnikov Institute of Radioengineering and Electronics of RAS, http://www.cplire.ru/
Moscow 125009, Russian Federation
E-mail: grachev@cplire.ru

Received July 04, 2023, peer-reviewed July 11, 2023, accepted July 18, 2023

Abstract: **Within the numerical experiment framework, the holographic processing of noise emission from a moving underwater sound source in the intense internal waves presence, which cause horizontal refraction of sound field waves, is considered. The interference of the undisturbed and disturbed fields forms a moiré interference pattern (interferogram) that masks the noise source interferogram. Registration of a moiré interferogram using a two-dimensional Fourier transform makes it possible to separate the spectral densities of the unperturbed and perturbed fields. This makes it possible to reconstruct the interferogram of the unperturbed field in the intense internal waves presence. The relative error of its reconstruction is estimated. The errors in reconstructing the range and source radial velocity due to horizontal refraction are analyzed.**

Keywords: **shallow sea, moving sound source, intense internal waves, horizontal refraction, interferogram, hologram**

UDC 004.052.34

Acknowledgments: The study was supported by the Russian Science Foundation grant No. 23-61-10024, https://rscf.ru/project/23-61-10024/. Numerical calculations of the sound field interferogram were carried out by S.A. Tkachenko with the support of the grant of the President of the Russian Federation MK-4846.2022.4.

For citation: Venedikt M. Kuz'kin, Sergey A. Pereselkov, Vladimir I. Grachev, Sergey A. Tkachenko, Nikolay V. Ladykin, Mikhail V. Kutsov. Holographic Method for Localization of a Moving Underwater Sound Source in the Intense Internal Waves Presence. *RENSIT: Radioelectronics. Nanosystems. Information Technology,* 2023, 15(3):317-326e. DOI: 10.17725/rensit.2023.15.317.

Contents

1. INTRODUCTION

Recently, of increasing interest in ocean acoustics are works on holographic interferometry using the two-dimensional Fourier transform (2D-FT) of the interferogram, which makes it possible to solve a wide range of new problems in the hydroacoustic information processing field [1-3]. An interferogram is understood as the modulus square of the received signal in frequency-time variables. The interferogram is characterized by a waveguide invariant [4], which determines the interference fringes slope. The slope establishes a relationship between the frequency shift of the interference maxima of the sound field and time (distance) while maintaining the phase difference between the interfering modes. The location geometry of the localized bands is determined by the waveguide parameters, the speed and trajectory of the sound source. At the output of the integral transformation (hologram), the spectral density is localized in a narrow band in the form of focal spots corresponding to the interference of different numbers modes. The hologram records the amplitudes of the interfering modes and the phase difference between them in all intermediate states that the source successively passes during the observation time.

In [1-3], it was assumed that the oceanic environment is homogeneous, i.e. its characteristics in the space-time domain are unchanged. In the hydrodynamic perturbations presence, the interferogram can be represented as the sum of the unperturbed and perturbed waveguide interferograms. The 2D-FT transformation is a linear process, which allows the hologram to be considered as a linear superposition of the unperturbed and perturbed waveguide holograms. If the spectral densities of the unperturbed and perturbed holograms are separated, then the inverse 2D-FT transformation to the selected spectral densities makes it possible to observe the unperturbed and perturbed fields interferograms.

For the first time, successful separation of the unperturbed and perturbed holograms was demonstrated by processing the data of the SWARM-95 full-scale experiment on stationary paths [5,6], when intense internal waves (IIWs) caused horizontal refraction and interaction of source acoustic field modes [7]. In [8,9], this effect was theoretically described and confirmed by the numerical simulation results, and the errors in reconstructing the unperturbed fields interferograms were estimated.

In this paper, generalizing the results of [8], within the numerical simulation framework, we consider the holographic processing of a moving source in the IIWs field, which determine the horizontal mode refraction. The IIWs effect on the error in reconstructing the distance, the radial velocity (velocity projection towards the receiver) of the source, and the interferogram of the undisturbed field is estimated.

2. EXPERIMENTAL CHARACTERISTICS OF INTENSE INTERNAL WAVES IN SHALLOW WATERS

Intense internal waves are a hydrodynamic phenomenon that is widespread in the oceanic environment. In shallow water areas, they are trains of intense short-period fluctuations of the constant density water surface, interpreted as solitons trains that propagate in the coastline direction. The reason for their occurrence is due to internal tides [10]. According to experimental data, soliton trains are characterized by the following parameters: velocity u ~ 0.5-1 m/s, periods of calm δL ~ 5-10 km, length L ~ 2-4 km, period D ~ 200-400 m (distance between crests of adjacent solitons), half-width η ~ 50-150

m, amplitude B ~ 10-30 m [11-13]. Soliton trains are characterized by: *a*) anisotropy in the horizontal plane, radius of front curvature r = 15-25 km; *b*) quasi-sinusoidality in the propagation direction, i.e. spatial narrow spectrum; *c*) synchronism of vertical displacements in depth, which indicates the dominance of the first gravity mode. These properties determine the horizontal refraction of source sound waves if the acoustic path is located at a small angle to the wave front of the soliton train [14,15].

3. DESCRIPTION OF INTENSE INTERNAL WAVES

Let us assume that the velocity of the soliton train is directed along the normal to the path located along the horizontal axis X. The soliton wavefront is assumed to be flat. In the absence of oceanic medium perturbation, the waveguide is considered to be horizontally homogeneous with depth H. Unperturbed values are denoted by an overline, and perturbed ones by a tilde. With the notation made, the refractive index square

$$n^2\left(x,y,z_q,t\right)=\overline{n}^2\left(z\right)+\tilde{n}^2\left(x,y,z,t\right), \quad (1)$$

where z_q is the receiver depth, t is time, and the y-axis is perpendicular to the x-axis (right-handed Cartesian coordinate system). The refractive index is understood as the ratio of the sound speeds on the surface z = 0 to the value of the sound speed at the depth under consideration. According to [16]

$$\tilde{n}^2\left(x,y,z_q,t\right)=-2QN^2\left(z_q\right)\left(z\right)\left(y,t\right). \quad (2)$$

Here $Q \approx 2.4$ s^2/m is a constant determined by the water physical properties; $N(z)$ is the buoyancy frequency; $\Phi(z)$ is the eigenfunction of the first gravity mode, normalized to the eigenvalue at the reception depth; $\zeta(y,t)$ is the deviation of the surface from the depth, where $\Phi(z)$ = 1. Due to the chosen geometry of the problem, the right side of expression (2) does not depend on the x coordinate. We write the envelope of the soliton train $\zeta(y,t)$ when crossing the path as a sequence of N different solitons with amplitudes B_n shifted relative to each other by a period D_n and propagating with velocities u_n

$$\varsigma\left(y,t\right)=\sum_{n=1}^{N}-B_n\operatorname{sech}^2\left[\left(y-D_n-u_nt\right)/\eta_n\right], \quad (3)$$

where η_n is the half-width of the n-th soliton at a level of 0.42 from the maximum [10]. The minus sign means that the perturbation of the refractive index is directed towards the bottom.

Taking into account the smallness $\tilde{n}^2$ with respect to $\overline{n}^2$, $\tilde{n}^2 \ll \overline{n}^2$, the real part of the horizontal wave number $h_m(x,z,t)$ (propagation constant) of the sound field of mode number m can be represented as

$$h_m\left(y,z,t\right)=\overline{h}_m+\tilde{h}_m\left(y,z,t\right), \quad (4)$$

where the linear correction within the framework of perturbation theory [14] is determined by the expression

$$\tilde{h}_m\left(y,z,t\right)=\frac{\overline{k}_0^2}{2\overline{h}_m}\int_0^H\overline{\Psi}_m^2\left(z\right)\tilde{n}^2\left(y,z,t\right)dz. \quad (5)$$

Here, $\overline{k}_0^2=\omega^2/\overline{c}_0^2$ is the squared wavenumber at depth z = 0, $\omega = 2\pi f$ is the cyclic frequency; $\overline{\Psi}_m(z)$ is the eigenfunction of the mth mode. Substituting (2) into (5), we obtain

$$\tilde{h}_m\left(y,z,t\right)=-q_m\varsigma\left(y,t\right), \quad (6)$$

where form

$$q_m=\frac{Q\overline{k}_0^2}{\overline{h}_m}\int_0^H\overline{\Psi}_m^2\left(z\right)N^2\left(z\right)\Phi\left(z\right)dz \quad (7)$$

is the dependence of the propagation constant linear correction on the mode number. The applicability limits of the perturbation method are limited by the solitons amplitudes on the order of several tens of meters, which are typical for shallow water areas [14].

4. HOLOGRAM FORMATION

The field of a broadband source is understood as the sound pressure in frequency-time variables. Let us write the radiation interferogram of a moving source as a modes sum

$$\begin{aligned} &I(\omega,t)= \\ &=\left|S(\omega)\right|^2\sum_m\sum_n A_m(\omega,\,t)\,A_n^*(\omega,\,t)\exp\left[ih_{mn}(\omega)(r_0+wt)\right]= \\ &=\sum_m\sum_n I_{mn}(\omega,t),\quad m\neq n. \end{aligned} \tag{8}$$

where $h_{mn}(\omega) = h_m(\omega) - h_n(\omega)$. Here $S(\omega)$ is the signal spectrum; $A_m(\omega,t)$ is the amplitude of the m-th mode; r_0 is the initial distance at time $t_0 = 0$, w is the source radial velocity. The superscript "*" denotes the complex conjugate value. Cylindrical divergence, modal attenuation, and source depths z_s and receivers z_q are taken into account in the mode amplitude. The modes number is M. The condition $m \neq n$ means that the mean value has been subtracted from the interferogram. If this operation is not performed before applying the 2D-FT transformation, then an intense peak will appear on the hologram at the coordinates origin.

Let us apply to the interferogram (8) the 2D-FT transformation

$$\begin{aligned} &F(\tau,\tilde{\nu})=\sum_m\sum_n\int_0^{\Delta t}\int_{\omega_1}^{\omega_2} I_{mn}(\omega,t)\exp\left[i(\tilde{\nu}t-\omega\tau)\right]dtd\omega= \\ &=\sum_m\sum_n F_{mn}(\tau,\tilde{\nu}). \end{aligned} \tag{9}$$

Here τ and $\tilde{\nu}=2\pi\nu$ are the time and circular frequency of the hologram; $\omega_{1,2} = \omega_0 \pm \Delta\omega/2$, $\Delta\omega$ is the band, ω_0 is the spectrum average frequency; Δt is the observation time. We restrict ourselves to the linear approximation of the waveguide dispersion

$$h_m(\omega)=h_m(\omega_0)+\frac{dh_m(\omega_0)}{d\omega}(\omega-\omega_0). \tag{10}$$

Assuming the amplitude spectrum of the signal $|S|$ and the amplitude A_m with frequency ω varying slowly compared to the rapidly oscillating factor $\exp[ih_m(\omega)(r_0 + wt)]$, for the partial hologram $F_{mn}(\tau,\tilde{\nu})$ (9) we obtain [2]

$$\begin{aligned} &F_{mn}(\tau,\tilde{\nu})= \\ &=\left|S(\omega_0)\right|^2 A_m(\omega_0)A_n^*(\omega_0)\Delta\omega\Delta t\exp\left[i_{mn}(\tau,\tilde{\nu})\right]\times \\ &\times\frac{\sin\left\{\left[r_0\dfrac{dh_{mn}(\omega_0)}{d\omega}-\tau\right]\dfrac{\Delta\omega}{2}\right\}}{\left[r_0\dfrac{dh_{mn}(\omega_0)}{d\omega}-\tau\right]\dfrac{\Delta\omega}{2}}\frac{\sin\left\{\left[wh_{mn}(\omega_0)+\tilde{\nu}\right]\dfrac{\Delta t}{2}\right\}}{\left[wh_{mn}(\omega_0)+\tilde{\nu}\right]\dfrac{\Delta t}{2}}, \end{aligned} \tag{11}$$

where is the phase

$$\Phi_{mn}(\tau,\tilde{\nu})=\left(\frac{\tilde{\nu}\Delta t}{2}-\tau\omega_0\right)+h_{mn}(\omega_0)\left(\frac{\Delta t}{2}w+r_0\right). \tag{12}$$

In (11) the approximation $r_0 \gg w\Delta t$.

Spectral density (9) is localized in two narrow regions in the form of focal spots. They are located: in the first and third quadrants, if the source approaches the receiver, $w < 0$; in the second and fourth quadrants, if the source moves away from the receiver, w > 0. The localization region contains $(M - 1)$ main maxima with coordinates $(\tau_\mu,\tilde{\nu}_\mu)$, located on a straight line $\tilde{\nu}=\tilde{\varepsilon}\tau$. Here, $\mu=\overline{1,M-1}$ is the focal spot number. At points with coordinates $(\tau_\mu,\tilde{\nu}_\mu)$ $(M - \mu)$ of the main peaks are summarized. The slope coefficient $\tilde{\varepsilon}=2\pi\varepsilon$ can also be represented in the form $\tilde{\varepsilon}=-\delta\omega/\Delta t$, where $\delta\omega$ is the frequency shift of the interferogram maximum over time δt. The linear dimensions of focal spots $\delta\tau$, $\delta\tilde{\nu}$ along the axes τ, $\tilde{\nu}$ do not depend on their numbers and are equal: $\delta\tau = 4\pi/\Delta\omega$, $\delta\tilde{\nu}=4\pi/\Delta t$ [2].

From the first focal spot closest to the origin, the radial velocity and initial distance are estimated as

$$\dot{w}=-\kappa_{w1}\tilde{\nu}_1,\quad \dot{r}_0=\kappa_{r1}\tau_1, \tag{13}$$

where

$$\begin{aligned} &\kappa_{w1}=(M-1)\left[h_{1M}(\omega_0)\right]^{-1}, \\ &\kappa_{r1}=(M-1)\left[dh_{1M}(\omega_0)/d\omega\right]^{-1}. \end{aligned} \tag{14}$$

The restored source parameters, in contrast to the true values, are indicated by a dot at the top.

Holographic processing is implemented as follows. During the observation time Δt in the emission band $\Delta\omega$, J independent realizations of duration t_1 with a time interval t_2 between them are quasi-coherently accumulated along the interference fringes: $J = \Delta t/(t_1 + t_2)$. Realizations are independent if $t_2 > 2\pi/\Delta\omega$. An interferogram $I(\omega,t)$ is formed and the 2D-FT transformation is applied to it.

In general, the transformation of a 2D-FT function is completely different from the function itself. However, a hologram is an unambiguous representation of an interferogram. The inversion, performed by inverse application of the 2D-FT transform, reconstructs the interferogram.

5. NUMERICAL SIMULATION

To be able to compare the holographic processing results for the cases of a stationary and moving source in the IIWs field, which determine the sound waves horizontal refraction, the simulation data are the same as in [8].

The depth distribution of the sound speed is shown in **Fig. 1**. Two frequency ranges were considered: f_1 = 100-120 Hz and f_2 = 300-320 Hz. Parameters of the liquid absorbing bottom: density ratio of soil and water ϱ = 1.8; for the first frequency range, the complex refractive index is $n = 0.84(1 + i0.03)$, for the second, $n = 0.84(1 + i0.05)$. In the f_1 frequency range, the field was formed by four modes, and in the f_2 frequency range, by ten modes. Mode propagation constants $h_m(\omega_0)$ and their frequency derivatives $dh_m(\omega_0)/d\omega$ at mid-range frequencies f_0 = 110, 310 Hz are given in **Tables 1, 2**.

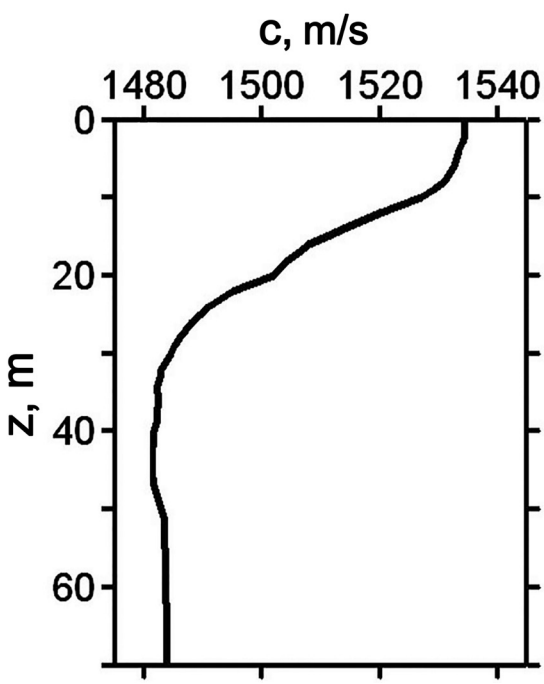

Fig. 1. *Unperturbed sound velocity profile.*

Table 1

Frequency f_0 = 110 Hz

Mod numbers, m	1	2	3	4
h_m, m^{-1}	0.4635	0.4557	0.4450	0.4310
$(dh_m/d\omega)\cdot10^{-4}$, s/m	6.7624	6.8085	6.9014	7.0912

Table 2

Frequency f_0 = 310 Hz

Mod numbers, m	1	2	3	4	5
h_m, m^{-1}	1.3123	1.3073	1.3006	1.2920	1.2826
$(dh_m/d\omega)\cdot10^{-4}$, s/m	6.7511	6.7619	6.7813	6.7973	6.8080
Mod numbers, m	6	7	8	9	10
h_m, m^{-1}	1.2730	1.2630	1.2525	1.2403	1.2258
$(dh_m/d\omega)\cdot10^{-4}$, s/m	6.8150	6.8312	6.8753	6.9703	7.0574

At the initial time $t_0 = 0$, the distance between the source and a single receiver x_0 = 10 km, the source approaches the receiver along the horizontal axis x. The source is located at a depth of z_s = 20 m, the receiver is at a depth of z_q = 45 m. The radial velocity of the source is $w = -1$ m/s. A uniform spectrum was set. Pulses with duration t_1 = 4 s (frequency sampling step 0.25 Hz) of sound pressure were recorded at intervals $t_* = 5$ s, ($t_* = t_1 + t_2$). As a perturbation model (3), we chose a train consisting of three identical solitons moving along the normal to the path. Soliton parameters: amplitude B = 20 m, width η = 200 m, velocity u = 0.7 m/s, period D = 250 m. The width of the perturbation front exceeds the path length. The observation time Δt = 20 min, during which time the soliton train completely crossed the path. With the chosen spectrum

model, the unperturbed field interferogram in the perturbation absence reproduces the transfer function of the waveguide up to a constant factor. The sound field at the receiving point was calculated using the approach of vertical modes and a parabolic equation in the horizontal plane [14].

The simulation results are shown in **Fig. 2-5**. The dotted line on the holograms shows the band in which the spectral density of the received signal is concentrated. Linear band dimensions: $\delta\tau \approx 0.15$ s, $\delta\nu \approx 0.002$ Hz, which agrees with the theoretical estimates of the sizes of focal spots $\delta\tau = 0.1$ s, $\delta\nu = 0.0017$ Hz [2].

On **Fig. 2** shows interferograms and moduli of unperturbed fields holograms in the absence of a path crossing by a solitons train. As the frequency increases, the irregularity of the interference pattern, which consists of localized inclined fringes, and the number of focal spots in the hologram increase, which is explained by an increase in the number of modes. Angular coefficients of interference fringes: $\delta f/\delta t \approx -0.015$ s^{-2} (frequency range f_1) and $\delta f/\delta t \approx -0.040$ s^{-2} (frequency range f_2).

Peak coordinates of the first focal spot: $\tau_1 = 1.30\cdot10^{-1}$ s, $\nu_1 = 1.79\cdot10^{-3}$ Hz (Δf_1); $\tau_1 = 4.08\cdot10^{-2}$ s, $\nu_1 = 1.54\cdot10^{-3}$ Hz (Δf_2). According to (15) and the data of Tables 1 and 2, the restored source parameters are:

$$\dot{w} = -1.0\ m/s,\ \dot{x}_0 = 11.8\ km\ (f_1);$$
$$\dot{w} = -1.0\ m/s,\ \dot{x}_0 = 12.0\ km\ (f_2).$$

Moiré interferograms and holograms modules when a solitons train crosses the path are shown in **Fig. 3**. Perturbation of the aquatic environment causes a change in the refractive index. This leads to a interference fringes transformation and a change in the configuration of the holograms spectral densities Moiré interferograms (Fig. 3*a,b*) show horizontal fringes with a width of $\Delta T_1 \approx 5.6$ min (f_1), $\Delta T_2 \approx 5.9$ min (f_2) with a quasi-periodic pattern of focal spots. Linear focal spots sizes: $\delta f_1 \approx 2.4$ Hz, $\delta t_1 \approx 1.1$ min (f_1) and $\delta f_2 \approx 2.8$ Hz, $\delta t_2 \approx 1.1$ min (f_2). Periodicity scales for focal spot maxima: $\delta\Lambda_1 \approx 5.6$ Hz, $\delta T_1 \approx 8.3$ min (f_1) and $\delta\Lambda_2 \approx 6.8$ Hz, $\delta T_2 \approx$

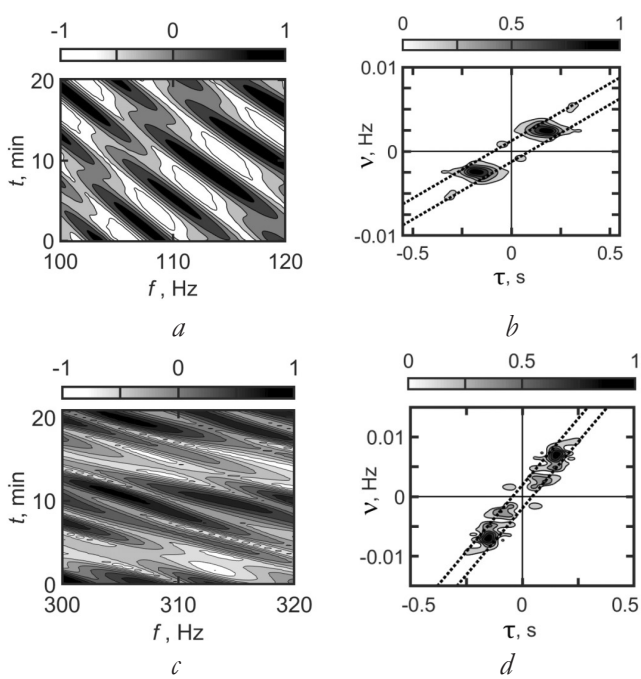

Fig. 2. *Normalized interferograms (a, c) and holograms (b, d) in the absence of perturbation: (a, b) – frequency range f_1, (c, d) – frequency range f_2.*

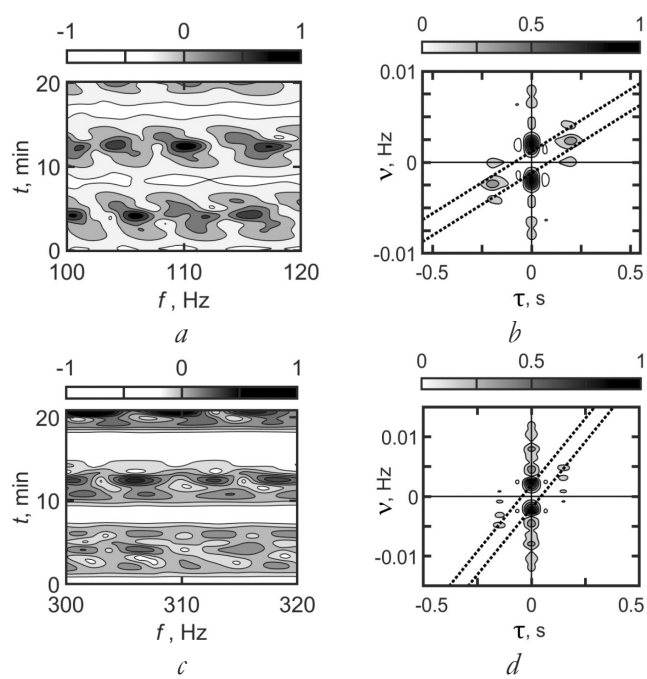

Fig. 3. *Normalized moiré interferograms (a, c) and holograms (b, d) in the presence of a disturbance: (a, b) – frequency range f_1, (c, d) – frequency range f_2.*

8.1 min (f_2). Although the values of the focal spots parameters in the interferograms are approximately the same as in the case of a stationary source, the interferograms noticeably differ in contrast and symmetry of the horizontal interference fringes arrangement [8]. In the holograms (Fig. 3*b,g*), the spectral density in the form of focal spots is concentrated mainly on the frequency axis, which gives an idea of the refracted signal influence.

In contrast to moiré interferograms, the location configuration of focal spots on holograms makes it possible to separately observe the spectral densities of the unperturbed and perturbed fields. The undisturbed and disturbed fields in the IIWs presence are understood to mean the fields formed by direct and refracted signals. Under natural conditions, when the train consists of solitons of different shapes and different parameters, this will naturally lead to a decrease in the contrast of the interference pattern and an expansion of the region of location of focal spots on the hologram.

The cleaning results the holograms spectral densities from the perturbed field in the frequency axis ν vicinity and their Fourier image are shown in **Fig. 4.** The shape of the spectral densities arrangement on the holograms of the unperturbed waveguide (Fig. 2*b,g*) and reconstructed in the IIWs presence (Fig. 4*b,g*) are close to each other. The peak coordinates of the first focal spot are estimated as follows: $\tau_1 = 1.50 \cdot 10^{-1}$ s, $\nu_1 = 2.05 \cdot 10^{-3}$ Hz (f_1); $\tau_1 = 4.08 \cdot 10^{-2}$ s, $\nu_1 = 1.54 \cdot 10^{-3}$ Hz (f_2). According to (15) and the data of Tables 1, 2, the restored source parameters

$$\dot{w} = -1.2\ m/s,\ \dot{x}_0 = 13.7\ km\ (f_1);$$
$$\dot{w} = -1.0\ m/s,\ \dot{x}_0 = 12.0\ km\ (f_2).$$

For the frequency range f_1, the perturbation leads to an increase in the error in restoring the source parameters;

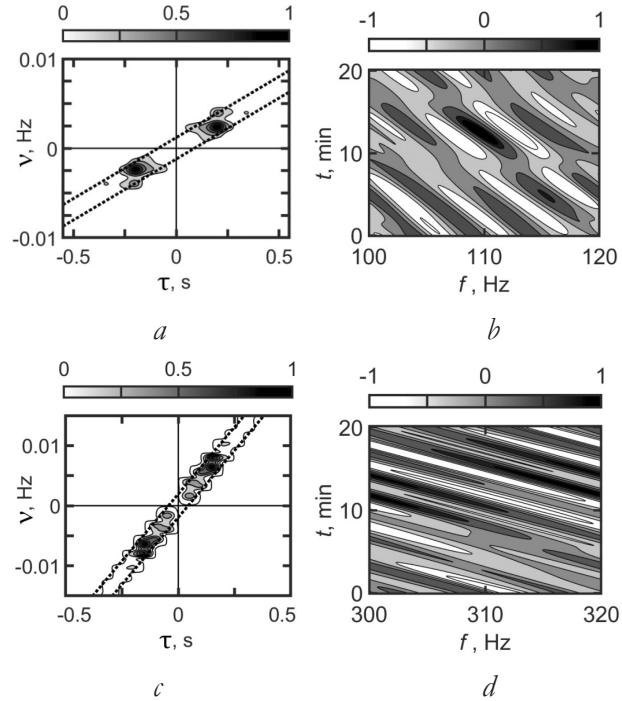

Fig. 4. *Normalized filtered modules of holograms (a, c) of the unperturbed field and interferograms (b, d) reconstructed from them: (a, b) – frequency range Δf_1, (c, d) – frequency range Δf_2.*

for the frequency range f_2, the perturbation presence does not affect the error in restoring the source parameters. This is explained by the increased influence of waves horizontal refraction on the formation of the source sound field with decreasing frequency [14]. The reconstructed interferograms of the unperturbed field in the presence of a train of solitons are shown in Fig. 4*b,d*. The angular coefficients of the interference fringes are estimated as $\delta f/\delta t \approx -0.017$ s^{-2} (Δf_1) and $\delta f/\delta t \approx -0.042$ s^{-2} (Δf_2), which is close to their values in the absence of medium disturbance.

The closeness degree of two-dimensional interferograms of unperturbed fields in the IIWs absence and presence will be estimated from the proximity of their one-dimensional interferograms, which are a horizontal section for a fixed time moment. With the chosen model of a uniform signal spectrum, one-dimensional interferograms, up to a constant factor, are equal to the transfer functions of

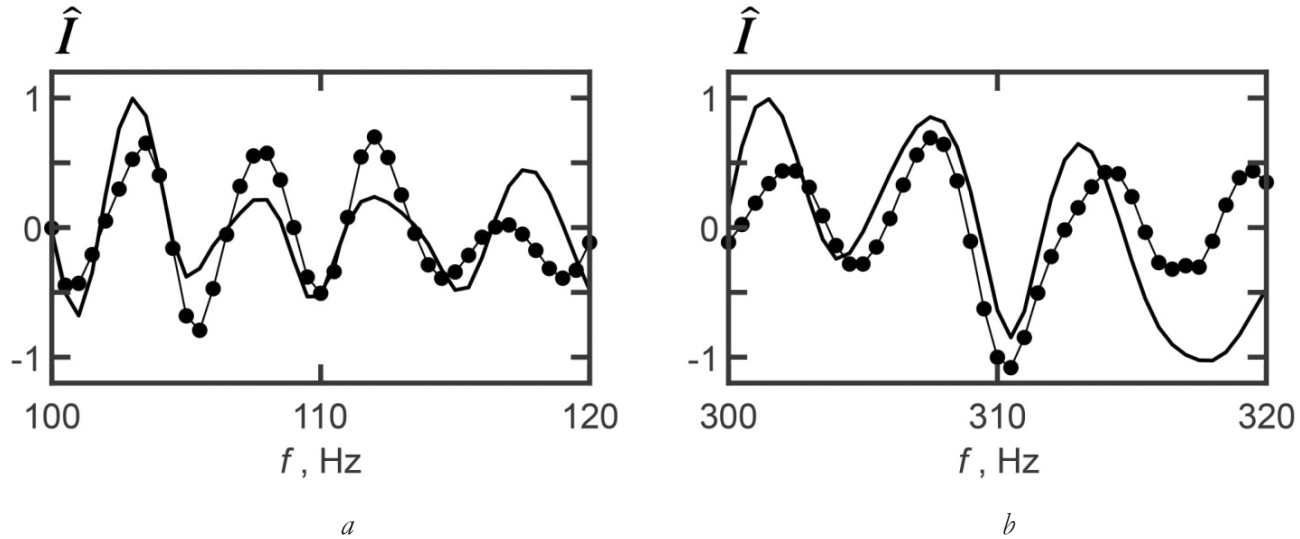

Fig. 5. *Dependences of normalized one-dimensional interferograms of unperturbed fields* $\hat{I}$ *on frequency f in the absence of a disturbance (solid line) and reconstructed in its presence (points): (a) frequency range* f_1*, (b) frequency range* f_2*.*

the waveguide in the absence and presence of a disturbance. On **Fig. 5** shows the one-dimensional normalized spectral densities of the unperturbed fields interferograms in the absence of a disturbance (solid line) and those reconstructed in its presence (points) for the time instant t = 10 min. The normalized value is indicated at the top with the "lid" icon. The error in reconstructing the interferograms was estimated as

$$d(t) = \frac{\sum_{j=1}^{J} \left| I_1(f_j, t) - I_2(f_j, t) \right|}{\sum_{j=1}^{J} \left| I_1(f_j, t) \right|}, \qquad (15)$$

where the readings number is J = 80. Here $I_{1,2}$ is the one-dimensional interferogram of the unperturbed field for time t in the disturbance absence and reconstructed in its presence, respectively. For the frequency range f_1, the error is d = 0.45; for the frequency range f_2, d = 0.60. Compared to a stationary source [8], the error increased by a factor of 3.7 and 6.2 for the frequency ranges f_1 and f_2, respectively. The indicated difference in the error values is explained by the different medium variability character. With a stationary source, there is a temporal variability of the medium, and with a moving source, there is a spatio-temporal variability. Note that the error (16) depends on the chosen moment of time.

6. CONCLUSION

Within the numerical simulation framework, the holographic method stability of localization of a moving broadband sound source in the IIWs presence, which determine the sound waves horizontal refraction, is demonstrated. The processing stability is based on the fact that the spectral densities of the unperturbed and perturbed fields do not overlap in the hologram, so that each of them can be observed separately. The filtering of these regions makes it possible, with minimal distortion, to reconstruct the unperturbed field hologram of a moving source in the IIWs presence in order to estimate its parameters. With an increase in the frequency range, the error in reconstructing the distance and the source radial velocity decreases. The inverse 2D-FT transformation application to the unperturbed hologram makes it possible to reconstruct the unperturbed field interferogram in the IIWs presence. The unperturbed field interferograms in

the absence and presence of IIWs differ in contrast, but their angular interference fringes coefficients are comparable in magnitude.

REFERENCES

1. Cockrell KL, Schmidt H. Robust passive range estimation using the waveguide invariant. *Acoust. Soc. Am.*, 2010, 127(5):2780-2789; https://doi.org/10.1121/1.3337223.
2. Kuznetsov GN, Kuz'kin VM, Pereselkov SA, Kaznacheev IV. Noise source localization in shallow water. *Phys. Wave Phenom.,* 2017, 25(2):156-163; https://doi.org/10.3103/S1541308X17020145.
3. Emmetiere R, Bonnel J, Gehant M, Cristol X, Chonavel T. Understanding deep-water striation patterns and predicting the waveguide invariant as a distribution depending on range and depth. *Acoust. Soc. Am.*, 2018, 143(6):3444-3454; https://doi.org/10.1121/1.5040982.
4. Chuprov SD. *Interference structure of a sound field in a layered ocean. Ocean Acoustics. Current State.* Moscow, Nauka Publ., 1982, pp. 71-91.
5. Apel J, Badiey M, Chiu C, Finette S, Headrick RH, Kemp J, Lynch J, Newhall A, Orr M, Pasewark B, Tielburger D, Turgut A, Heydt KVD, Wolf S. An overview of the SWARM 1995 shallow-water internal wave acoustic scattering experiment. *IEEE J. Ocean. Eng.*, 1997, 22:465-500; https://doi.org/10.1109/48.611138.
6. Frank SD, Badiey M, Lynch J, Siegmann W. Analysis and modeling of broadband airgum data influenced by nonlinear internal waves. *J. Acoust. Soc. Am.*, 2004, 116(6):3404-3422; https://doi.org/10.1121/1.1819499.
7. Badiey M, Kuz'kin VM, Pereselkov SA. Interferometry of hydrodynamics of oceanic shelf caused by intensive waves. *Fundam. Prikl. Gidrofiz.*, 2020, 13(1):45-55; https://doi.org/10.7868/S2073667320010050.
8. Kaznacheeva ES, Kuz'kin VM, Pereselkov SA. Interferometric processing of hydroacoustic information in the presence of intense internal waves. *Phys. Wave Phenom.*, 2021, 29(3):278-284; https://doi.org/10.3103/S1541308X21030067.
9. Kuz'kin VM, Lyakhov GA, Pereselkov SA, Kaznacheeva ES. The information transmission through random-inhomogeneous ocean environment. *Fundam. Prikl. Gidrofiz.,* 2021, 14(2):54-64; https://doi.org/10.7868/S2073667321020052.
10. Konyae KV, Sabinin KD. *The Waves within the Ocean.* St. Petersburg, Gidrometeoizdat Publ., 1992.
11. Zhou J, Zhang XZ, Rogers PH. Resonant interaction of sound wave with internal solitons in the coastal zone. *Acoust. Soc. Am.*, 1991, 90(4):2042-2053; https://doi.org/10.1121/1.401632.
12. Hsu MK, Liu AK, Liu C. An study of internal waves in the China seas and yellow sea using SAR. *Continental Shelf Research*, 2000, 20(4-5):389-410; https://doi.org/10.1016/S0278-4343(99)00078-3.
13. Li X, Clemente-Colon P, Friedman KS. Estimating jceanic mixed-layer depth from internal wave evolution observed from Radarsat-1 SAR. *Johns Hopkins APL Technical Digest.*, 2000, 21(1):130-135.
14. Katsnel'son BG, Pereselkov SA. Low-frequency horizontal acoustic refraction caused by internal wave solitons in a shallow sea. *Acoust. Phys.* 2000, 46(6):684-691; https://doi.org/10.1134/1.1326723.

15. Oba R, Finette S. Acoustic propagation through anisotropic internal wave fields: transmission loss, cross-range coherence, and horizontal refraction. *Acoust. Soc. Am.*, 2002, 111(2):769-784; https://doi.org/10.1121/1.1434943.

16. Flatte SM (ed.). *Sound transmission through a fluctuating ocean*. Cambridge University Press, 1979, 299 p.